THEORETICAL AND APPLIED MECHANICS
Volume 45 (2018) Issue 2, 231–251 DOI: https://doi.org/10.2298/TAM180819013S

ANALYSIS OF DYNAMICS VARIATION AGAINST THIXOTROPIC PARAMETER'S PREFERENTIAL RANGE

Nazish Shahid

Abstract. Variation in the dynamics of a steady-state blood flow through a stenosed tapered artery has been investigated corresponding to changes in thixotropic parameter λ over the range [0,1]. To probe the role of parameter λ and differentiate the current model from other known non-Newtonian models, expressions of axial velocity, shear stress, wall shear stress and flow rate have been calculated depending upon this parameter and pressure gradient. Also, pressure gradient has been deduced uniquely with the help of the continuity equation. Our choice of calculating pressure gradient has led to obtaining shear stress such that its dependence on the structural parameter of our model, unlike most available results, motivates for further investigation. The simultaneous effects of varying yield stress and parameter λ on axial velocity, flow resistance and flow rate have been studied such that the differences between the Herschel–Bulkley fluid model and our current model can be pointed out. To validate the suitability of our model and some results in history, we have also obtained limiting results for particular values of λ.

1. Introduction

An arterial stenosis has not only been known to cause malfunction in the vascular system, but disruption in smooth supply of blood also compromises the life span of organs. A subject of such critical importance has been given due attention and a good number of experimental and theoretical investigations have been devoted to understanding arterial rheology and its mechanism. Various methods and compatible models have been adopted to describe flow propagation through a stenosed artery, which has helped to understand the dynamical differences caused by parameter variations or change in systems conditions, etc. Choosing different models to describe this sort of flow has also facilitated simulation of these systems. Early investigations [1–3] regarding flow characteristics in a tube and extension of this work to variation in dynamics due to change in time inspired and motivated efforts for further probe. Elshehawey et al, Shahed and Sharma et al. [4–6] contributed to the analysis of pulsatile flow through stenosed and porous mediums

2010 *Mathematics Subject Classification:* 76A05; 76D99; 76Z05; 65H04; 65K05; 37M05.
Key words and phrases: thixotropy, tapering, blood flow, steady-state, axial velocity, yield stress.

along with effects of body acceleration, periodic body acceleration and transverse magnetic field.

Much experimental and theoretical work [7–15] was devoted to the study of these systems based on the classification of fluid flowing in a channel depending on viscosity, geometry of channels, elasticity and tapering of vessels. A numerical probe by Long et al. [16] helped to understand the physiological angle of pulsatile flow through arterial stenosis. The limitation of flow through a severely constricted symmetric tube was highlighted by Smith [17]. Deshpande et al. and Mandal et al. [18, 19] differentiated the dynamics in steady flow in vascular stenoses and unsteady flow through a stenosed artery, respectively.

Lack of Newtonian fluid modelling to consider some characteristics of fluid such as change of viscosity in time, among many, motivated the researchers to probe results of blood flow through stenosis using non-Newtonian fluid modelling. Many interesting aspects of arterial flow were investigated by characterising blood as non-Newtonian fluid using the Power-law model, Casson model and Harshel-Bulkley model [20–31]. In [32–34], the characteristics of blood, shear thinning and varying level of viscoplasticity, etc., were highlighted in the context of blood flow propagation through a constricting tube. On the basis of the pattern of red blood cell aggregation in the form of rouleaux structure and its disintegration due to flow, the suitability of Casson and Herschel–Bulkley models was discussed in detail in [35–37]. Working on the subject of blood flow through a stenosed artery, Priyadharshini et al. discussed the dynamics of flow in the context of movement of the artery wall and the factor of dilation using Herschel–Bulkley model [38]. The role of time parameter in the dynamics of blood flow due to bifurcating movements of vessels was investigated in [39–41].

Recently [42–44], some efforts have been invested in describing the characteristics of yield stress and time-dependent viscosity by linking these characteristics with a structural parameter of modelling of the relevant system. In those works, system's evolution is discussed in the context of parameter's evolution such that the parameter satisfies a relaxation equation. But, some questions regarding the effectiveness of this model in comparison to Casson and Harshel-Bulkley models are yet to be answered. However, some experimental works [45,46] on arterial rheology suggested the suitability of the Casson model only for low shear-rate scenarios and its limitation in dealing with some phenomenal characteristics of blood.

Following an experimental insight of Apostolidis [47] where a model with a combination of yield stress and shear rate, linked with a structural parameter, is suggested to better describe both low shear and transient shear phenomena, we have extended our investigation based on this model's construction. Here, we have probed the role and capacity of this model's parameter to influence the physiological and rheological characteristics. For our model describing the steady-state flow of blood through a constricted channel with tapering, we have determined the analytical expressions of axial velocity, shear stress, wall shear stress and flow rate depending upon pressure gradient. A unique numerical approach to deducing pressure gradient has been adopted such that it can be incorporated to analyse other physical quantities. The effects of variation in structural parameter and varying

yield stress on the system evolution have also been quantified. Some important conclusions have been reached through graphical illustrations. A range of structural parameter variation has been suggested over which experimental axial velocity seems to get closer to our model's velocity than the velocity value obtained through other known non-Newtonian models.

2. Flow Geometry

A system of unsteady, incompressible and non-Newtonian fluid flow through a blood vessel with mild stenosis and tapering has been represented with the help of a cylindrical coordinate system $(r,\ \theta,\ z)$ where the directions of r, z and θ are taken to be along the radius of a vessel, axis of channel or artery and along the circumferential direction, respectively. We have adopted Thixotropic modelling to describe the two-dimensional flow through an arterial segment with stenosis. The flow geometry has been described as [41]

$$\bar{R}(z) = \begin{cases} \Big((m'z + R_0) - \frac{\gamma_{m'} \sec\varphi(z-d)}{\frac{l_0^2}{4} - \gamma_{m'}^2 \sin^2\varphi}(l_0 - (z-d))\Big), & \text{for } d \leqslant z \leqslant d + l_0 \\ (m'z + R_0), & \text{otherwise} \end{cases}$$

where $\bar{R}(z)$, l_0, d, R_0, φ have been used to denote the radius of a tapered artery in the stenotic region, length of stenosis, position of stenosis, constant radius of non-tapered artery in the non-stenotic region and angle of tapering, respectively. The notions of converging tapering, diverging tapering and no tapering have been represented by $\varphi < 0$, $\varphi > 0$ and $\varphi = 0$, respectively. For the slope of tapering and height of stenosis with no tapering at $z = d + \frac{l_0}{2}$, the notations of $m' = \tan\varphi$ and $\gamma_{m'}$ have been used.

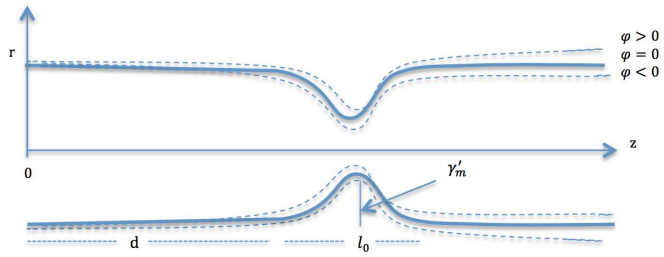

FIGURE 1. A tapering channel in 2-D with stenosis

3. Mathematical modelling

We describe the axisymmetric flow in the stenosed vessel using momentum equations corresponding to r-component and z-component and the continuity equation as following

$$\rho\Big(\frac{\partial u}{\partial t} + u\frac{\partial u}{\partial r} + w\frac{\partial u}{\partial z}\Big) = -\Big(\frac{1}{r}\frac{\partial(r\tau_{rr})}{\partial r} + \frac{\partial(\tau_{zr})}{\partial z}\Big) - \frac{\partial p}{\partial r},$$

$$\rho\Big(\frac{\partial w}{\partial t}+u\frac{\partial w}{\partial r}+w\frac{\partial w}{\partial z}\Big)=-\Big(\frac{1}{r}\frac{\partial(r\tau_{rz})}{\partial r}+\frac{\partial(\tau_{zz})}{\partial z}\Big)-\frac{\partial p}{\partial z},$$
$$\frac{\partial u}{\partial r}+\frac{u}{r}+\frac{\partial w}{\partial z}=0,$$

where u and w are radial and axial components of velocity, and ρ denotes the density of flow. The constitutive equations have corresponding to structural parametric model equation has been considered as

$$\tau=\lambda\tau_y+(1-\lambda)\bar{k}(-\dot{\gamma})^n,\quad \tau>\tau_y$$

such that $\tau=|\tau_{rz}|=-\tau_{rz}$. And

$$\dot{\gamma}=0,\quad \tau\leqslant\tau_y.$$

In our model, λ has been used as a structural parameter varying over the range $(0,1)$. Also, τ, τ_y, $\dot{\gamma}$, n and $\bar{k}$ are shear stress, yield stress, rate of deformation, index of flow behaviour and consistency index, respectively.

The boundary conditions are

$$u=0,\quad w=0\ \text{ at }\ r=\bar{R};\qquad \tau_{rz}=0\ \text{ at }\ r=0.$$

The following choice of non-dimensional variables has been opted for to simplify the problem that is

$$\begin{aligned}
&u^*=\frac{u}{u_0}, && w^*=\frac{w}{w_0}, && t^*=\frac{w_0t}{l}, && z^*=\frac{z}{l}, && p^*=\frac{p}{p_0},\\
&w_0=\frac{u_0l}{R_0}, && t_0=\frac{l}{w_0}, && K=\frac{\bar{k}}{\mu}\Big(\frac{w_0}{R_0}\Big)^{n-1}, && \tau^*_{rz}=\frac{R_0\tau_{rz}}{\mu w_0}, &&\\
&\tau^*_{zz}=\frac{l\tau_{zz}}{\mu w_0}, && p_0=\frac{\mu l w_0}{R_0^2}, && R^*=\frac{\bar{R}}{R_0}, && d^*=\frac{d}{l}, && l_0^*=\frac{l_0}{l},\\
&\omega^*=\frac{t_0\omega}{2\pi}, && m=\frac{m'l}{R_0}, && \gamma^*_{m'}=\frac{\gamma_{m'}}{R_0}, && \tau^*_y=\frac{R_0\tau_y}{\mu w_0}, &&\\
&\tau^*_{rr}=\frac{R_0\tau_{rr}}{\mu u_0}, && r^*=\frac{r}{R_0}, && Q^*=\frac{\bar{Q}}{w_0R_0^2}, && \mathrm{Re}=\frac{\rho R_0w_0}{\mu}. &&
\end{aligned}\tag{3.1}$$

Using Eq. (3.1), very small Reynolds number, Re, and $R_0\ll l$ where l represents the finite length of artery and ignoring $*$, we get our system simplified as

$$-\frac{\partial p}{\partial z}=\frac{1}{r}\frac{\partial(r\tau_{rz})}{\partial r},\tag{3.2}$$

$$\frac{\partial p}{\partial r}=0,\tag{3.3}$$

$$\tau=\lambda\tau_y+(1-\lambda)K\Big(-\frac{\partial w}{\partial r}\Big)^n,\tag{3.4}$$

$$\frac{\partial u}{\partial r}+\frac{u}{r}+\frac{\partial w}{\partial z}=0,\tag{3.5}$$

with boundary conditions

$$u(r,z)=0,\quad w(r,z)=0\ \text{ at }\ r=R(z);\qquad \tau_{rz}(r,z)=0\ \text{ at }\ r=0.\tag{3.6}$$

Also, the wall geometry is

$$R(z) = \Big\{(mz+1) - \frac{4\gamma_m \sec\varphi (z-d)(l_0-(z-d))}{l_0^2}\Big\},$$

for $d \leqslant z \leqslant d + l_0$.

4. Analytical expressions of velocity and wall shear stress

Integrating Eq. (3.5) with respect to r from $r = 0$ to $r = R(z)$ and using boundary condition $(3.6)_1$, we obtain

$$\frac{\partial}{\partial z}\int_0^{R(z)} rw(r,z)dr = 0. \tag{4.1}$$

We use $x = \frac{r}{R(z)}$ for coordinate transformation and obtain from Eqs. (3.2), (3.3), (3.4) and (4.1) the following

$$-\frac{\partial p}{\partial z} = \frac{1}{xR(z)}\frac{\partial (x\tau_{xz})}{\partial x}, \tag{4.2}$$

$$-\frac{\partial p}{\partial x} = 0, \tag{4.3}$$

$$\tau = \lambda\tau_y + \frac{(1-\lambda)K}{R^n(z)}\Big(-\frac{\partial w}{\partial x}\Big)^n, \tag{4.4}$$

$$\frac{\partial}{\partial z}\Big(R^2(z)\int_0^1 xw(x,z)dx\Big) = 0, \tag{4.5}$$

with boundary conditions

$$w(x,z) = 0 \quad \text{at} \quad x = 1; \qquad \tau_{xz}(x,z) = 0 \quad \text{at} \quad x = 0. \tag{4.6}$$

We, also, have

$$\frac{\partial w}{\partial x} = 0, \quad 0 \leqslant x \leqslant R_{\rm pc}$$

where $R_{\rm pc}$ is the radius of the plug core region.

With the help of Eqs. (4.2) and (4.3), we can write pressure gradient as a function of only an axial coordinate that is

$$p = p(z). \tag{4.7}$$

Solving Eq. (4.2) with $(4.6)_2$ and (4.7), we obtain an expression of shear stress

$$\tau_{xz} = \frac{xR(z)}{2}\Big(-\frac{\partial p}{\partial z}\Big). \tag{4.8}$$

And the expression for wall shear stress $(x = 1)$ is

$$\tau_{ws} = \frac{R(z)}{2}\Big(-\frac{\partial p}{\partial z}\Big). \tag{4.9}$$

Solving Eq. (4.4) with $(4.6)_1$ and (4.8),we get an expression for axial velocity

$$w(x,z) = \frac{nR(z)}{(n+1)(M+2\lambda\tau_y)(2K(1-\lambda))^{\frac{1}{n}}}\Big\{M^{\frac{n+1}{n}} - \big(Mx + 2\lambda\tau_y(x-1)\big)^{\frac{n+1}{n}}\Big\}, \tag{4.10}$$

where $M = R(z)(-\frac{\partial p}{\partial z}) - 2\lambda\tau_y$ and $R_{\rm pc} \leqslant x \leqslant R(z)$.

And the velocity of fluid in the plug core region is

$$w_{pc}(x,z) = \frac{nR(z)}{(n+1)(M+2\lambda\tau_y)(2K(1-\lambda))^{\frac{1}{n}}}\{M^{\frac{n+1}{n}}\},$$

for $0 \leqslant x \leqslant R_{\rm pc}$ and $R_{\rm pc} = \frac{2\lambda\tau_y}{R(z)-\frac{\partial p}{\partial z}}$.

Volume flow-rate is defined as

$$\bar{Q} = 2\pi \int_{r=0}^{r=\bar{R}(z)} rw(r,z)dr,$$

which in non-dimensional form (ignoring $*$) can be written as

$$Q(z) = 2\pi \int_{r=0}^{r=R(z)} rw(r,z)dr. \tag{4.11}$$

Eq. (4.11) in terms of x coordinate is

$$Q(z) = 2\pi R^2(z) \int_0^1 xw(x,z)dx. \tag{4.12}$$

5. Numerical analysis of pressure gradient

We have to find an expression for pressure gradient. Using Eqs. (4.5) and (4.12), we can write

$$Q = 2\pi\ R^2(z) \int_0^1 xw(x,z)dx = C, \tag{5.1}$$

where C is a constant. Simplifying Eq. (5.1), we obtain

$$\begin{aligned} Q = {} & \frac{\pi nR^3(z)}{(n+1)(2n+1)(3n+1)(M+2\lambda\tau_y)^3(2K(1-\lambda))^{\frac{1}{n}}} \\ & \times \Big\{(n+1)(2n+1)M^{\frac{3n+1}{n}} + 4\lambda\tau_y(n+1)(3n+1)M^{\frac{2n+1}{n}} \\ & + 4\lambda^2\tau_y^2(2n+1)(3n+1)M^{\frac{n+1}{n}}\Big\} = C, \end{aligned} \tag{5.2}$$

where M is defined as $M = R(z)\big(-\frac{\partial p}{\partial z}\big) - 2\lambda\tau_y$.

Choosing $C = 1$, Eq. (5.2) has been numerically solved using MATLAB for the values of pressure gradient, $-\frac{\partial p}{\partial z}$. These pressure gradient values can further be used to evaluate shear stress (4.8), wall shear stress (4.9) and axial velocity (4.10).

Resistance to flow can be obtained using

$$\mho = \int_0^z \frac{\big(-\frac{\partial p}{\partial z}\big)}{Q}dz,$$

with the help of Eqs. (4.12) and (5.2).

For converging tapering, we have constructed Table 1 to study the changes in pressure gradient according to changes in yield stress and parameter λ at a position of stenosis, $z = 28$. Consistently with phenomenal experimental findings [48],

TABLE 1. Values of pressure gradient $-\frac{\partial p}{\partial z}$ for varying yield stress, $z = 28$ and λ

	$\boldsymbol{\lambda = 0.1}$	$\boldsymbol{\lambda = 0.5}$	$\boldsymbol{\lambda = 0.7}$
$\boldsymbol{\tau_y}$	$\boldsymbol{-\frac{\partial p}{\partial z}}$	$\boldsymbol{-\frac{\partial p}{\partial z}}$	$\boldsymbol{-\frac{\partial p}{\partial z}}$
0.05	14.0215	7.8799	4.8091
0.1	14.0418	7.9813	4.9507
0.4	14.1635	8.5880	5.7962
0.8	14.3258	9.3931	6.9102
1.2	14.4879	10.1935	8.0092
1.6	14.6498	10.9892	9.0946
2.0	14.8118	11.7802	10.1680
2.4	14.9735	12.5666	11.2309

pressure gradient is increasing with increase in yield stress. Also, it is noted that pressure gradient decreases with increase in λ-values. Additionally, we observe that the change in pressure gradient corresponding to the change in yield stress for Thixotropic model for $\lambda = 0.1$ tends to match with the results in the case of Herschel–Bulkley's model [38] but for our choice of consistency index value. Thus, we have deduced that parameter λ influences the arterial flow and plays its role in causing changes in dynamics in addition to the role of varying yield stress of fluid.

6. Discussion

We have used the following numerical figures [41] to study the dynamics of our Thixotropic system through graphs

$$R_0 = 0.8, \quad n = 0.639, \quad d = 20, \quad \gamma_m = 0.32, \quad \omega = 6$$
$$g = 0.1, \quad \tau_y = 0.4, \quad K = 1.6, \quad l = 50, \quad l_0 = 16.$$

The response of shear stress corresponding to the change in radial distances has been expressed in Figures 2 to 4. The values of shear stress have been obtained for the case of converging, diverging and no-tapering at a position of stenosis, $z = 28$. These graphs show that shear stress continues to increase while approaching the boundary wall of the vessel ($x = 1$) where it obtains its maximum absolute value. We observe that shear stress assumes higher values for converging tapering than for no tapering and diverging tapering, later assuming the smallest values. The fact that a constricted channel, in comparison to a straight or diverging channel, requires higher pressure gradient for a fixed amount of entering fluid helps to increase shear exercised on the wall of the vessel. These graphs have also been plotted to study the influence of thixotropic parameter λ on shear. It shows that shear stress increases for smaller values of λ (say $0 < \lambda \leqslant 0.5$) and decreases for larger values of λ. [h!]

Figures 5 to 7 represent variation in axial velocity at a position of stenosis, $z = 28$ for corresponding changes in near-wall radial distances. The response of axial velocity has been measured for converging, diverging and no-tapering. This graphical analysis shows that the axial velocity continues to decrease till it reaches

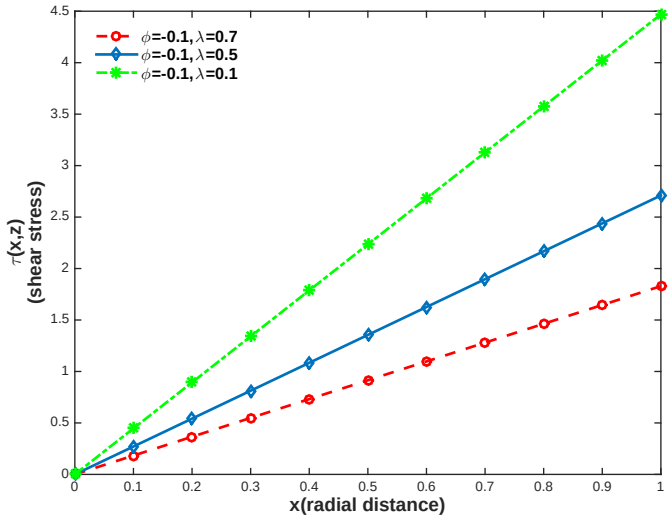

FIGURE 2. Shear stress vs radial distances for $\phi = -1$ at $z = 28$, $\tau_y = 0.4$, $K = 1.6$, $\boldsymbol{\lambda = 0.7, 0.5, 0.1}$

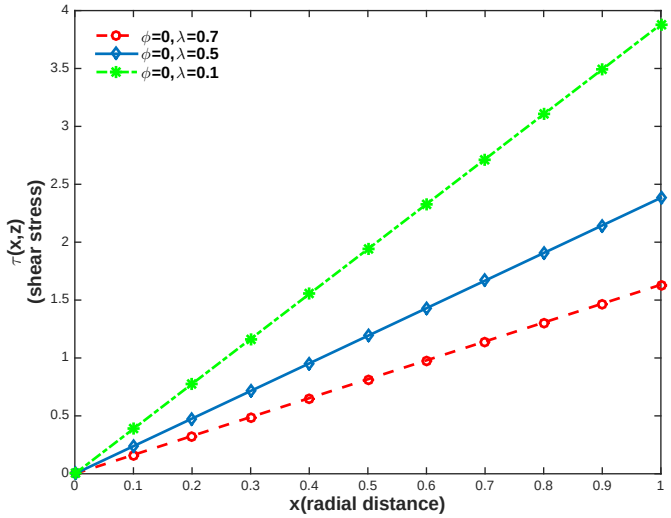

FIGURE 3. Shear stress vs radial distances for $\phi = 0$ at $z = 28$, $\tau_y = 0.4$, $K = 1.6$, $\boldsymbol{\lambda = 0.7, 0.5, 0.1}$

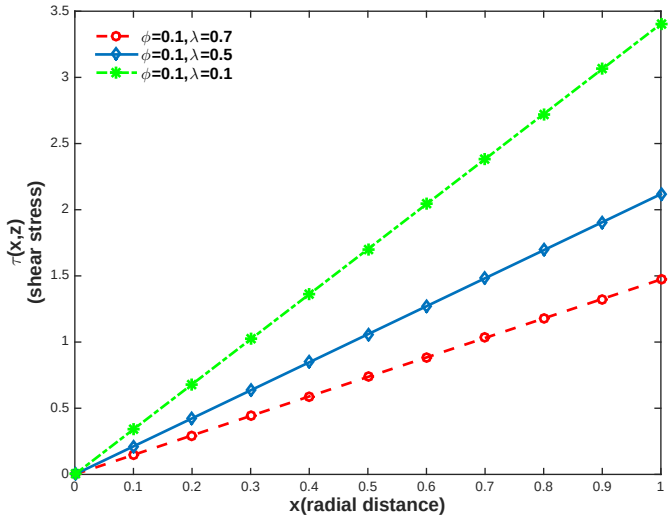

FIGURE 4. Shear stress vs radial distances for $\phi = 0.1$ at $z = 28$, $\tau_y = 0.4$, $K = 1.6$, $\boldsymbol{\lambda = 0.7, 0.5, 0.1}$

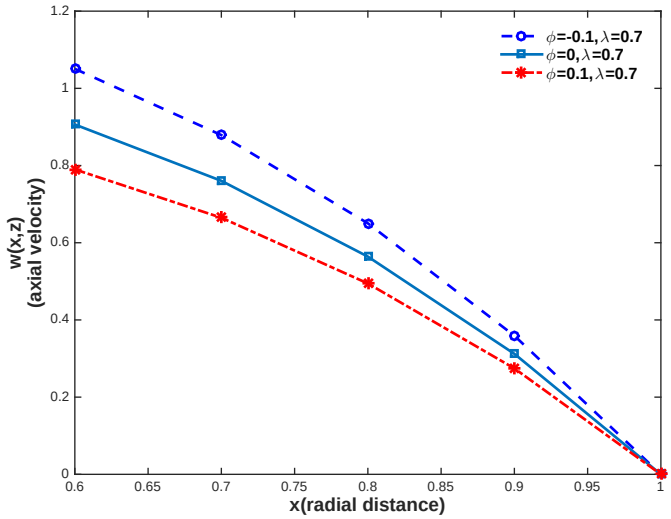

FIGURE 5. Axial velocity vs radial distances for $\phi = -1$, 0, 0.1 at $z = 28$, $\tau_y = 0.4$, $K = 1.6$, $\boldsymbol{\lambda = 0.7}$

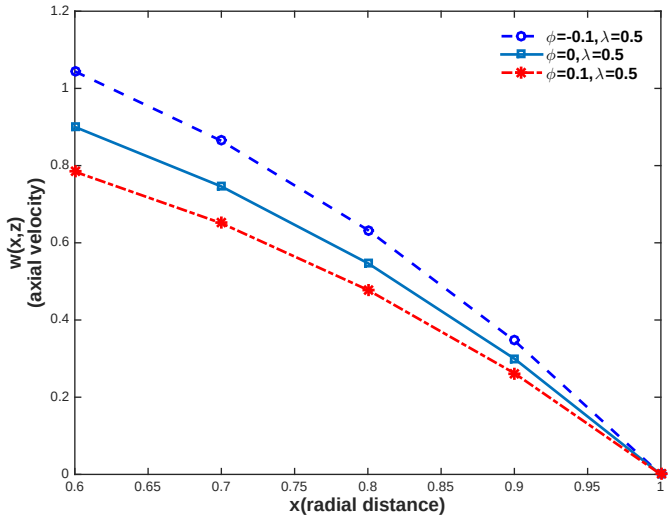

FIGURE 6. Axial velocity vs radial distances for $\phi = -1,\ 0,\ 0.1$ at $z = 28,\ \tau_y = 0.4,\ K = 1.6,\ \boldsymbol{\lambda = 0.5}$

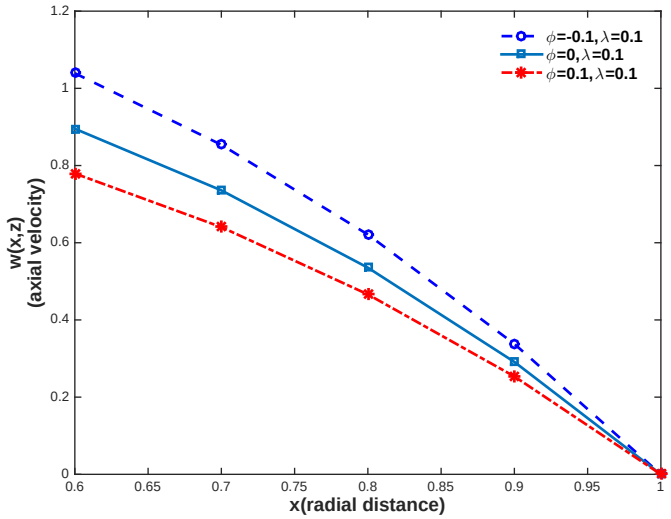

FIGURE 7. Axial velocity vs radial distances for $\phi = -1,\ 0,\ 0.1$ at $z = 28,\ \tau_y = 0.4,\ K = 1.6,\ \boldsymbol{\lambda = 0.1}$

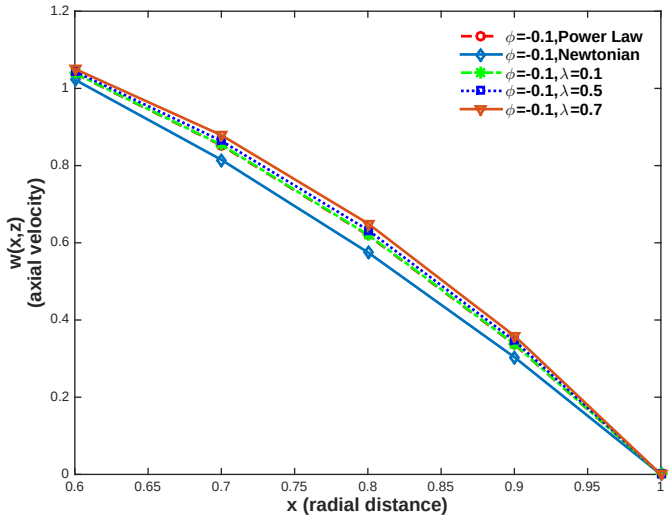

FIGURE 8. Axial velocity vs radial distances (near the wall) for $\phi = \mathbf{-0.1}$, $\boldsymbol{\lambda = 0.7,\ 0.5,\ 0.1}$ at $z = 28$, $\tau_y = 0.4$, $K = 1.6$, Power Law model ($\boldsymbol{\lambda \to 0}$) and Newtonian fluid ($\boldsymbol{\lambda \to 0}$, $\boldsymbol{\bar{K} = 0.035}$, $\boldsymbol{n = 1}$).

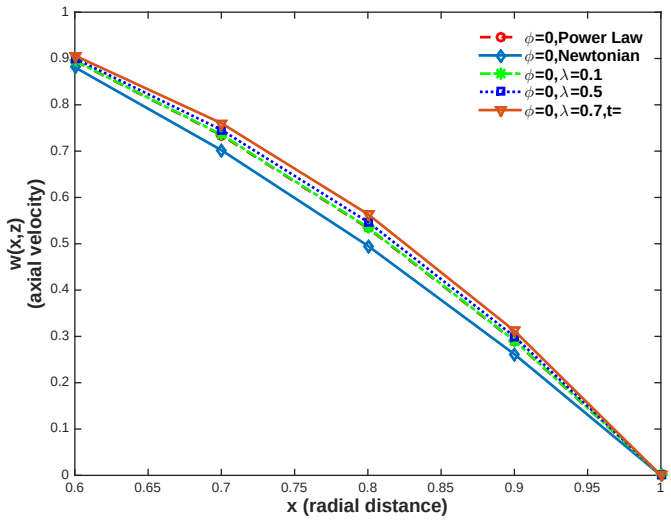

FIGURE 9. Axial velocity vs radial distances (near the wall) for $\boldsymbol{\phi = 0}$, $\boldsymbol{\lambda = 0.7,\ 0.5,\ 0.1}$ at $z = 28$, $\tau_y = 0.4$, $K = 1.6$, Power Law model ($\boldsymbol{\lambda \to 0}$) and Newtonian fluid ($\boldsymbol{\lambda \to 0}$, $\boldsymbol{\bar{K} = 0.035}$, $\boldsymbol{n = 1}$).

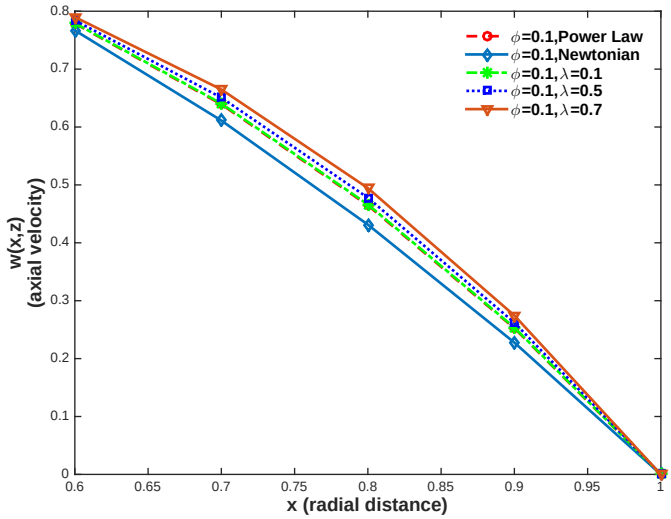

FIGURE 10. Axial velocity vs radial distances (near the wall) for $\boldsymbol{\phi = 0.1}$, $\boldsymbol{\lambda = 0.7, 0.5, 0.1}$ at $z = 28$, $\tau_y = 0.4$, $K = 1.6$, Power Law model ($\boldsymbol{\lambda \to 0}$) and Newtonian fluid ($\boldsymbol{\lambda \to 0}$, $\boldsymbol{\bar{K} = 0.035}$, $\boldsymbol{n = 1}$).

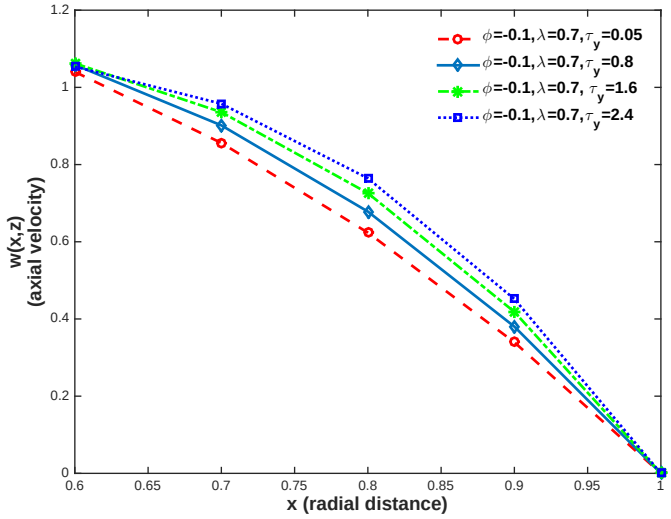

FIGURE 11. Axial velocity vs radial distances for $\boldsymbol{\phi = -0.1}$ at $z = 28$, $\boldsymbol{\tau_y = 0.05, 0.8, 1.6, 2.4}$, $K = 1.6$, $\boldsymbol{\lambda = 0.7}$

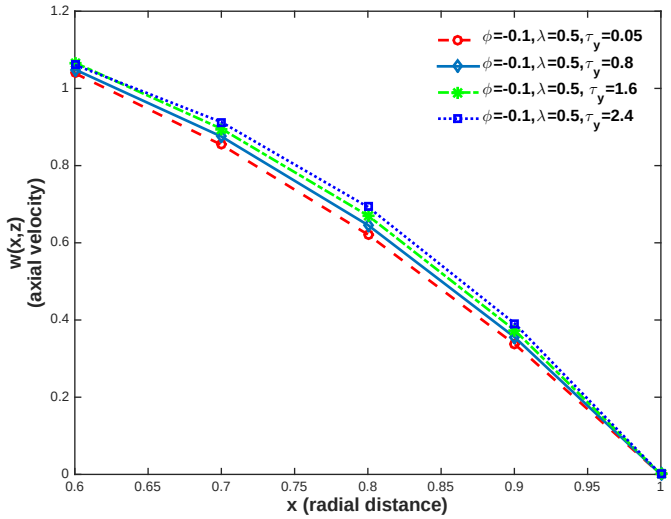

FIGURE 12. Axial velocity vs radial distances for $\boldsymbol{\phi = -0.1}$ at $z = 28$, $\boldsymbol{\tau_y = 0.05, 0.8, 1.6, 2.4}$, $K = 1.6$, $\boldsymbol{\lambda = 0.5}$

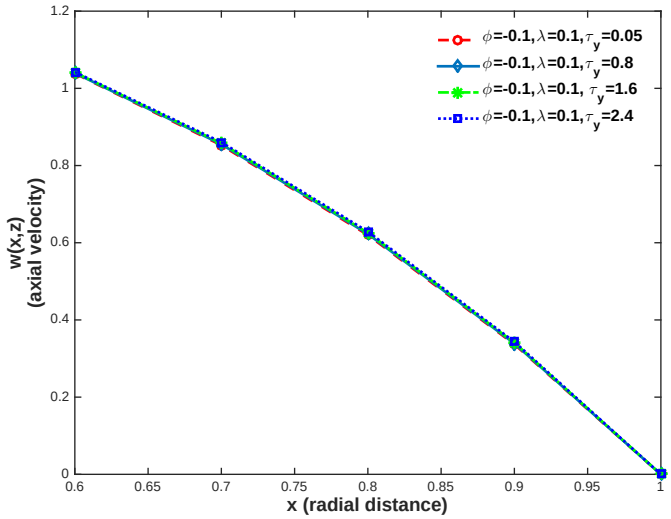

FIGURE 13. Axial velocity vs radial distances for $\boldsymbol{\phi = -0.1}$ at $z = 28$, $\boldsymbol{\tau_y = 0.05, 0.8, 1.6, 2.4}$, $K = 1.6$, $\boldsymbol{\lambda = 0.1}$

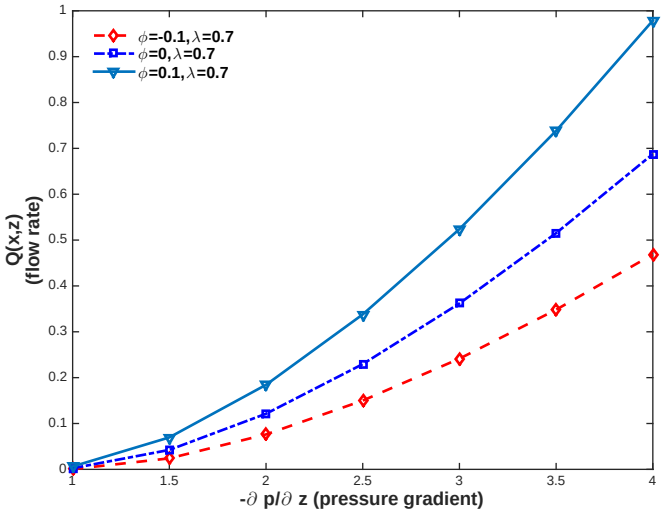

FIGURE 14. Flow rate vs pressure gradient $\phi = -0.1,\ 0,\ 0.1$ at $z = 28$, $\tau_y = 0.4$, $K = 1.6$, $\boldsymbol{\lambda = 0.7}$

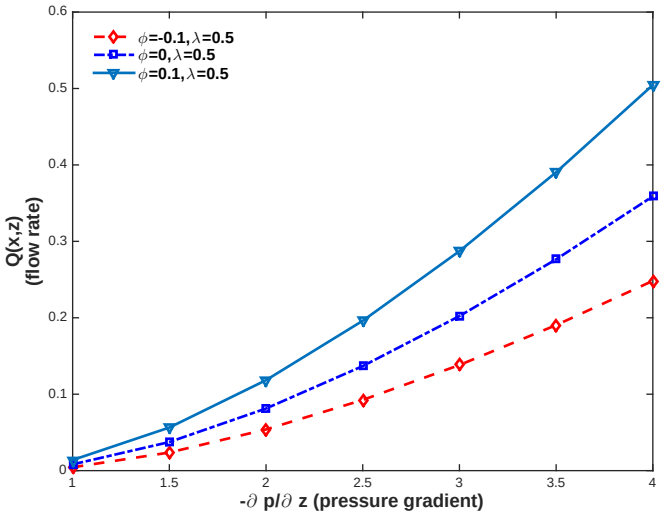

FIGURE 15. Flow rate vs pressure gradient $\phi = -0.1,\ 0,\ 0.1$ at $z = 28$, $\tau_y = 0.4$, $K = 1.6$, $\boldsymbol{\lambda = 0.5}$

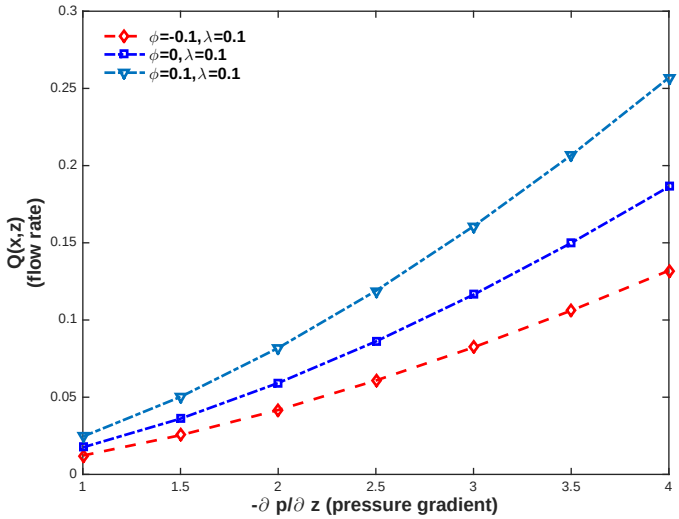

FIGURE 16. Flow rate vs pressure gradient $\boldsymbol{\phi = -0.1,\ 0,\ 0.1}$ at $z = 28$, $\tau_y = 0.4$, $K = 1.6$, $\boldsymbol{\lambda = 0.1}$

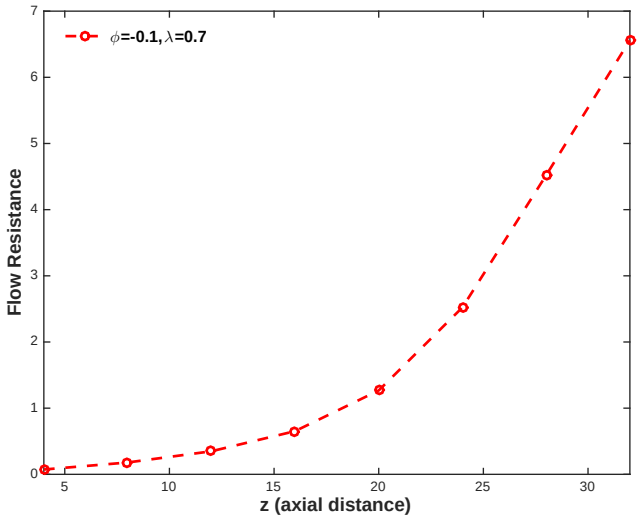

FIGURE 17. Flow rate vs pressure gradient $\boldsymbol{\phi = -0.1}$, $\tau_y = 0.4$, $K = 1.6$, $\boldsymbol{\lambda = 0.7}$

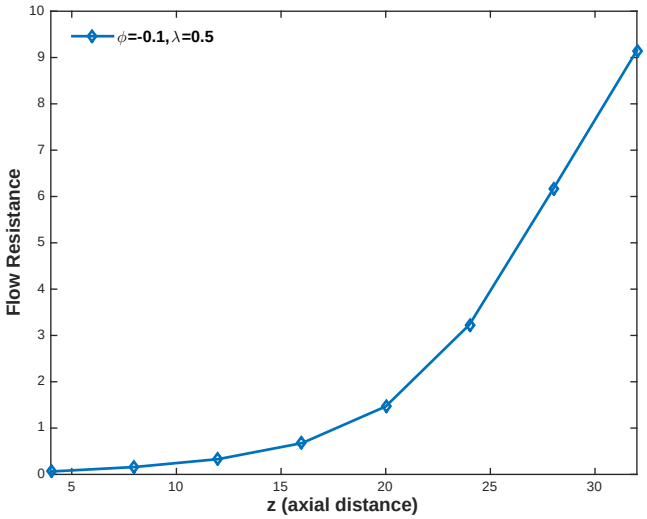

FIGURE 18. Flow rate vs pressure gradient $\boldsymbol{\phi = -0.1}$, $\tau_y = 0.4$, $K = 1.6$, $\boldsymbol{\lambda = 0.5}$

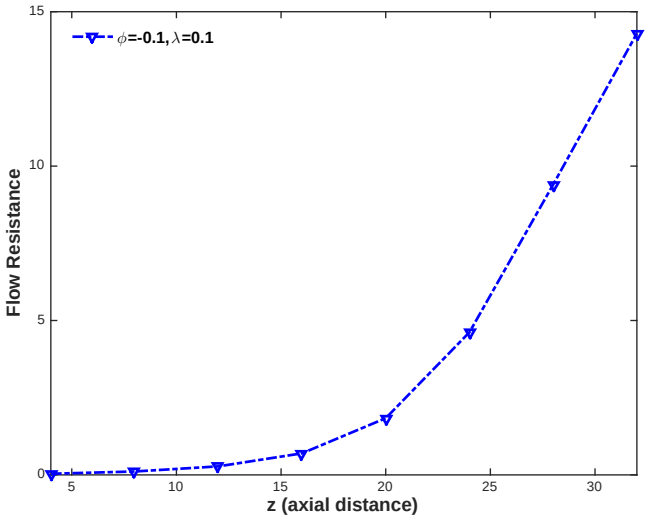

FIGURE 19. Flow rate vs pressure gradient $\boldsymbol{\phi = -0.1}$, $\tau_y = 0.4$, $K = 1.6$, $\boldsymbol{\lambda = 0.1}$

zero on the wall of the vessel, satisfying the no-slip boundary condition. Also, the magnitude of velocity for converging tapering is higher in comparison to not-tapered and diverging tapering in respective order. This phenomenon is also linked with the scenario of highest shear stress for converging tapering as higher pressure gradient in this case accelerates the fluid propagation, thus increasing the velocity of fluid. A slow decrease in axial velocity can also be observed as thixotropic parameter's values decrease.

In Figures 8 to 10, we have studied multiple profiles of axial velocity corresponding to Power law, Newtonian and thixotropic fluid ($\lambda = 0.1, 0.5, 0.7$) in response to a change in near-wall radial distances at a position of stenosis, $z = 28$ such that the velocity profiles can be compared and analysed. These graphs show that the Newtonian fluid assumes the smallest of magnitudes for axial velocity and is represented through the profile below all profiles. It can be seen that as value of λ increases, the magnitude of velocity also increases. Hence the profile for highest λ (here $\lambda = 0.7$) is appearing on top of all. Also, the profile for Power law fluid is above Newtonian fluid but it seems to be coinciding (more accurately closer to the vessel wall) with the axial velocity profile for $\lambda = 0.1$.

Figures 11 to 13 have been drawn to analyse the response of axial velocity at a position of stenosis for varying yield stress. These graphs have been plotted against changes in near-wall radial distances for the case of converging tapering. It is observed that axial velocity increases with increase in yield stress as higher yield stress fluid requires higher pressure gradient for flow propagation that in turn increases the velocity. It is interesting to note the influence of λ, thixotropic parameter, on velocity along with changes in yield stress. It is observed that as the velocity of λ decreases, even the change in yield stress does not affect the velocity profiles. This fact is apparent in Figure 13 where velocity profiles for yield stresses $\tau_y = 0.05, 0.8, 1.6, 2.4$ coincide for parametric value, $\lambda = 0.1$.

The variation of flow rate corresponding to changes in pressure gradient have been depicted through Figures 14 to 16. These figures have been obtained for the case of converging, diverging and no-tapering at the position of stenosis, $z = 28$. These figures express that the flow rate increase is non-linear corresponding to steady increase in pressure gradient unlike the available results in history for non-Newtonian fluid models where flow rate increases linearly with increase in pressure gradient. However, it can be observed that for smaller values of λ, the flow rate profiles start assuming an almost linear relation with pressure gradient. It is also noted that the flow rate magnitude is higher for diverging tapering in comparison to not-tapered and converging tapering in the respective order. In general, the relation of flow rate with parameter λ has been observed to be direct, that is, flow rate increases for increasing values of λ and vice versa.

Figures 17 to 19 represent a change in flow resistance with increasing axial distances for converging tapering. These graphs show that resistance to flow increases non-linearly and continuously with increase in axial distance. Due to constriction around $20 \leqslant z \leqslant 30$, a sharp increase in flow resistance is also observed. In these figures, the influence of parameter λ on flow resistance has also been studied. An inverse relation of flow resistance and parameter λ has been another interesting

observation, that is, the flow resistance increases considerably for smaller values of λ in the range $15 \leqslant z \leqslant 30$.

7. Conclusions

We have studied the changes in velocity, flow rate, shear stress and flow resistance due to changes in the structural parameter where this parameter is varying over a certain range. The following highlights have been made regarding the differences in dynamics due to the choice of our model and its suitability for encompassing the characteristics of blood flowing through a stenosed artery. The differences between our model and other non-Newtonian models have been particularly pointed out.

1. Shear stress continues to increase with increase in the radial distance, reaching its absolute maximum value on the boundary of the vessel.

2. For converging tapering, the absolute values of shear stress are higher in comparison to no-tapering and diverging tapering.

3. It was, interestingly, noted that higher λ (say $0.5 < \lambda < 1$) influences the flow in a way that shear stress is reduced in comparison to smaller λ-values' case.

4. Axial velocity continues to drop corresponding to an upward movement of the radial distance towards the wall of the channel where it assumes zero value, confirming the no-slip boundary condition.

5. Axial velocity assumes highest values for converging tapering and it decreases slowly with decrease in λ-values.

6. A study of multiple velocity profiles corresponding to Newtonian, Power law and thixotropic fluid ($\lambda = 0.1, 0.5, 0.7$) reveals that Newtonian fluid velocity assumes smallest values as compared to Power-law and thixotropic fluid velocities. However, the velocity profiles for Power-law fluid coincide with thixotropic fluid for $\lambda = 0.1$. The highest velocity magnitude is assumed by thixotropic fluid for highest λ-value (here), that is $\lambda = 0.7$. It appears that increasing λ-values causes hinderance in the propagation of non-Newtonian fluid flow that requires higher pressure gradient, thus increasing the velocity.

7. The highest axial velocity for converging tapering is also verified in comparative graphs.

8. A rise in yield stress of fluid causes the axial velocity to increase due to higher pressure gradient required for higher yield-stress fluid propagation. Interestingly, parameter λ influences the axial velocity in a way that for smaller λ-values the difference in velocity magnitude corresponding to varying yield stress is negligible (here $\lambda = 0.1$).

9. Flow rate continues to rise observing a slightly parabolic path with increase in pressure gradient such that flow rate magnitude for diverging tapering is higher in comparison to converging and no-tapering.

10. Parameter λ influences the flow rate directly corresponding to changes in pressure gradient. Also, flow rate assumes a linear relation with pressure gradient for $\lambda = 0.1$.

11. For converging tapering, resistance to flow continues to increase non-linearly with increasing axial distance, rising sharply in the vicinity of stenosis.

In a manner of validating a direct relation of flow rate with λ, here flow resistance has an inverse relation with λ. Thus, flow resistance decreases for higher λ-values and vice-versa.

References

1. D. F. Young, *Effect of a time dependent stenosis of flow through a tube*, Journal of Engineering for Industry **90** (1968), 248–254.
2. D. F. Young, F. Y. Tsai, *Flow characteristics in models of arterial stenoses: I. Steady flow*, Journal of Biomechanics **6** (1973), 395–410.
3. D. F. Young, *Fluid mechanics of arterial stenoses*, Journal of Biomechanical Engineering **101** (1979), 157–175.
4. E. F. Elshehawey, E. M. Elbarbary, N. A. S. Afifi, M. El-Shahed, *Pulsatile flow of blood through a porous medium under periodic body acceleration*, Int. J. Theor. Phys. **39** (2000), 183–188.
5. M. El-Shahed, *Pulsatile flow of blood through a stenosed porous medium under periodic body acceleration*, Appl. Math. Comput. **138** (2003), 479–488.
6. M. K. Sharma, K. Bansal, S. Bansal, *Pulsatile unsteady flow of blood through porous medium in a stenotic artery under the influence of transverse magnetic field*, Korea-Australia Rheology Journal **24** (2012), 181–189.
7. K. Imaeda, F. O. Goodman, *Analysis of nonlinear pulsatile blood flow in arteries*, Journal of Biomechanics **13** (1980), 1007–1022.
8. E. Belardinelli, S. Cavalcanti, *A new nonlinear two- dimensional model of blood motion in tapered and elastic vessels*, Computers in Biology and Medicine **21** (1991), 1–13.
9. J. C. Misra, S. Chakravarty, *Flow in arteries in the presence of stenosis*, Journal of Biomechanics **19** (1986), 907–918.
10. R. E. Nerem, *Vascular fluid mechanics, the arterial wall and arteriosclerosis*, Journal of Biomechanical Engineering **114** (1992), 274–282.
11. C. Tu, M. Deville, L. Dheur, L. Vandershuren, *Finite element simulation of pulsatile flow through arterial stenosis*, Journal of Biomechanics **25** (1992), 1141–1152.
12. M. Siouffi, V. Deplano, R. Pelissra, *Experimental analysis of unsteady flows through a stenosis*, Journal of Biomechanics **31** (1997), 11–19.
13. S. Cavalcanti, *Hemodynamics of an artery with mild stenosis*, Journal of Biomechanics **28** (1995), 387–399.
14. G. R. Zendehboodi, M. S. Moayeri, *Comparison of physiological and simple pulsatile flows through stenosed arteries*, Journal of Biomechanics **32** (1999), 959–965.
15. S. Chakravarty, P. K. Mandal, *Two-dimensional blood flow through tapered arteries under stenotic conditions*, Int. J. Non-Linear Mech. **35** (2000), 779–793.
16. Q. Long, X. Y. Ku, K. V. Ramnarine, P. Hoskins, *Numerical investigation of physiologically realistic pulsatile flow through arterial stenosis*, Journal of Biomechanics **34** (2001), 1229–1242.
17. F. T. Smith, *The separation flow through a severely constricted symmetric tube*, J. Fluid Mech. **90** (1979), 725–754.
18. M. D. Deshpande, P. D. Giddens, F. R. Mabon, *Steady laminar flow through modelled vascular stenoses*, Journal of Biomechanics **9** (1976), 165–174.
19. P. K. Mandal, S. Chakravarty, A. Mandal, N. Amin, *Effect of body acceleration on unsteady pulsatile flow of non-Newtonian fluid through a stenosed artery*, Appl. Math. Comput. **189** (2007), 766–779.
20. D. Liepsch, S. T. Moravec, *Pulsatile flow of non-Newtonian fluid in distensible models of human arteries*, Biorheology **21** (1984), 571–586.
21. G. Theodorou, D. Bellet, *Laminar flows of a non-Newtonian fluid in mild stenosis*, Comput. Methods Appl. Mech. Eng. **54** (1986), 111–123.
22. P. Chaturani, R. P. Samy, *A study of non-Newtonian aspects of blood flow through stenosed arteries and its applications in arterial diseases*, Biorheology **22** (1985), 521–531.
23. M. Nakamura, T. Swada, *Numerical study on the flow of a non-Newtonian fluid through an axisymmetric stenosis*, Journal of Biomechanical Engineering **110** (1988), 137–143.

24. S. Chakravarty, *Effects of stenosis on the flow behaviour of blood in an artery*, Int. J. Eng. Sci. **25** (1987), 1003–1016.
25. M. Nakamura, T. Swada, *Numerical study on the unsteady flow of non-Newtonian fluid*, Journal of Biomechanical Engineering **112**(1) (1990), 100–103.
26. B. Pak, Y. I. Young, S. U. S. Choi, *Separation and re-attachment of non-Newtonian fluid flows in a sudden expansion pipe*, J. Non-Newtonian Fluid. Mech. **37** (1990), 175–199.
27. P. Ponalagusamy, *Mathematical analysis on effect of non-Newtonian behavior of blood on optimal geometry of microvascular bifurcation system*, J. Franklin Inst. **349** (2012), 2861–2874.
28. P. Ponalagusamy, *Pulsatile flow of Herschel–Bulkley fluid in tapered blood vessels*, Proc. Int. Conf. Sci. Comp. World Cong. Computer Sci., Computer Eng., App. Comp. (2013), 67–73.
29. J. C. Misra, M. K. Patra, S. C. Misra, *A non-Newtonian fluid model for blood flow through arteries under stenotic conditions*, Journal of Biomechanics **26** (1993), 1129–1141.
30. C. Tu, M. Deville, *Pulsatile flow of non-Newtonian fluid through arterial stenosis*, Journal of Biomechanics **29** (1996), 899–908.
31. B. Das, P. C. Johnson, A. S. Popel, *Effect of non axisymmetric hematocrit distribution on non-Newtonian blood flow in small tubes*, Biorheology **35**(1) (1998), 69–87.
32. E. W. Merrill, *Rheology of blood*, Physiol. Rev. **49** (1969), 863–888.
33. G. R. Cokelet, E. W. Merrill, E. R. Gilliland, H. Shin, A. Britten, E. R. Wells, *The rheology of human blood Measurement near and at zero shear rate*, Trans. Soc. Rheology **7** (1963), 303–317.
34. L. Dintenfass, *Thixotropy of blood and proneness to thrombus formation*, Circulation Research **11**(2) (1962), 233–239.
35. G. W. Scott Blair, D. C. Spanner, *An Introduction to Biorheology*, Elsevier Scientific Publishing, Amsterdam, 1974.
36. B. Pincombe, J. Mazumdar, I. Hamilton-Craig, *Effects of multiple stenoses and post-stenotic dilatation on non- Newtonian blood flow in small arteries*, Medical & Biological Engineering & Computing **37** (1999), 595–599.
37. R. G. Owens, *A new micro structure-based constitutive model for human blood*, J. Non-Newton. Fluid Mech. **140** (2006), 57–70.
38. S. Priyadharshini, R. Ponalagusamy, *Biorheological model on flow of Herschel–Bulkley fluid through a tapered arterial stenosis with dilatation*, Applied Bionics and Biomechanics **2015** (2015), ID 406195, 12 pages.
39. M. J. Manton, *Low Reynolds number flow in slowly varying axisymmetric tubes*, J. Fluid Mech. **49** (1971), 451–459.
40. R. L. Whitemore, *Rheology of circulation*, Pergamon Press, Oxford, 1968.
41. P. K. Mandal, *An unsteady analysis of non-Newtonian blood flow through tapered arteries with a stenosis*, Int. J. Non-Linear. Mech. **40** (2005), 151–164.
42. A. Mujumdar, N. B. Anthony, A. B. Metzner, *Transient phenomena in thixotropic systems*, J. Non-Newton. Fluid Mech. **102** (2002), 157–178.
43. K. Dullaert, J. Mewis, *A structural kinetics model for thixotropy*, J. Non-Newton. Fluid Mech. **139** (2006), 21–30.
44. J. Mewis, N. J. Wagner, *Colloidal suspension rheology*, Cambridge Univ., Cambridge, 2012.
45. J. Mewis, *Thixotropy: A general review*, J. Non-Newton. Fluid Mech. **6** (1979), 1–20.
46. A. J. Apostolidis, N. B. Anthony, *Modelling of the blood rheology in steady-state shear flows*, J. Rheol. **58** (2014), 607–633.
47. A. J. Apostolidis, M. J. Armstrong, N. B. Anthony, *Modelling of human blood rheology in transient shear flows*, J. Rheol. **59** (2015), 275–298.
48. C. E. Huckaba, A. W. Hahn, *A generalised approach to the modeling of arterial blood flow*, Bull. Math. Biophys. **30** (1968), 645–662.

АНАЛИЗА ДИНАМИЧКЕ ВАРИЈАЦИЈЕ У ОДНОСУ НА ПРЕТПОСТАВЉЕН ИНТЕРВАЛ ТИСКОТРОПНОГ ПАРАМЕТРА

Резиме. Испитана је варијација динамике протока стационарног крвног тока кроз стенозирану артерију која одговара променама тискотропног параметра λ у интервалу [0,1]. Да би испитали улогу параметра λ и разликовали дати модел од других познатих не-Њутновских модела, у зависности од овог параметра и градијента притиска израчунати су изрази аксијалне брзине, напона смицања, напрезања зидова и промене тока. Такође, изведен је градијент притиска помоћу једначине континуитета.

Наш избор израчунавања градијента притиска омогућио нам је добијање напона смицања тако да његова зависност од структурног параметра модела, за разлику од већине расположивих резултата, мотивише даља истраживања. Истовремени ефекти варирања напона смицања и параметра λ на аксијалној брзини, отпорности тока и брзини тока су проучавани тако да се могу истаћи разлике између Herschel–Bulkley-овог и нашег модела флуида. Да бисмо потврдили валидност нашег модела у односу на неке познате резултате, такође смо добили граничне резултате за одређене вредности параметра λ.

Department of Mathematics
Forman Christian College
A Chartered University
Lahore
Pakistan
nash_shhd@hotmail.com
nazishshahid@fccollege.edu.pk

(Received 19.08.2018.)
(Revised 29.09.2018.)
(Available online 28.11.2018.)